High-energy x-ray emission in vacuum spark discharge

Han S. Uhm

Naval Surface Warfare Center, White Oak, Silver Spring, Maryland 20903-5000

Tong Nyong Lee

Department of Physics, Pohang Institute of Science and Technology, Pohang 790-600, Korea
(Received 14 March 1989)

A theory of the magnetic field diffusion is developed in order to explain high-energy x-ray emission observed in vacuum spark plasmas. The acceleration mechanism is based on the intense induced electric field due to an abrupt inductance change when the plasma column expands from its pinch radius to a large radius. According to this magnetic field diffusion model, high-energy electrons are well collimated at the axis. In addition, the electron energy in this collimated flux can be easily more than 20 times the electrode voltage, which generates high-energy x-ray radiation by interaction with the dense plasma.

I. INTRODUCTION

A vacuum spark microplasma emits strong line radiation arising from K transitions in He- and H-like ions of high Z (such as Fe) atoms and bremsstrahlung radiation, both of which are expected from a multi-keV temperature plasma. In addition, the discharge emits unexpectedly strong high-energy x rays associated with the microplasma formation. The photon energy of such radiation far exceeds the values expected from either the thermal bremsstrahlung or the applied electrode voltage.

Recently, Veretennikov et al.[1] have reported a very important piece of information regarding the time correlation between plasma dynamics and the formation of the microplasma. According to their multiple-frame, short-exposure-time shadow graphs, the microplasma is produced some time after (average of about 20 ns) the maximum contraction of the plasma column, as it expanded to a diameter of about 2 mm, contrary to what one might expects from any existing model. In order to explain this dilemma, they speculated that there may exist a second contraction immediately following the first, due to a radiation cooling, which is so fast that one could not normally observe it. It is well established that the final contraction to a microsize plasma is probably due to a plasma collapse[2] caused by a rapid radiation loss. However, exactly how the expanding plasma leads to the second collapse and emission of the high-energy x ray has not been well understood.

In order to explain these complex physical phenomena, we introduce a magnetic field diffusion model after expansion. In Sec. II, we develop a theoretical model based on the plasma expansion following the plasma pinch with minimum radius. Once the plasma column expands abruptly, the magnetic field stored inside the pinched plasma diffuses, thereby creating an intense induced electric field [Eq. (18)], which in turn accelerates charged particles into a very-high-energy state. This induced electric field is strongly concentrated at the axis [Eq. (19)]. The induced plasma current, which is proportional to the induced electric field, is also well collimated at the axis [Eqs. (5) and (18)]. This highly collimated electron flux interacts with the dense anode plasma, thereby creating high-density microplasma. Note that the electrons in the induced plasma current may have very high energy, which can be easily more than 20 times the electrode voltage. In Sec. III, the electron-energy spectrum and the corresponding x-ray spectrum are obtained for the magnetic diffusion model and numerical examples are presented. A qualitative discussion of the vacuum spark physics is presented in Sec. IV.

II. THEORETICAL MODEL

The theoretical model in this section is based on the plasma expansion scheme after a pinch state, which is schematically presented in Fig. 1. Here, axial distance of the pinch region is d_p, and the original pinch and new expanded radii are denoted by R_p and R_0, respectively. The plasma current I_0 is assumed to be constant. During contraction of the plasma column, the system inductance
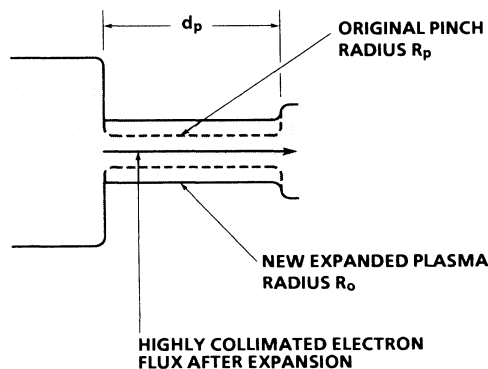

FIG. 1. Schematic presentation of a vacuum discharge plasma and the highly collimated electron beam at the axis.

increases, thereby storing magnetic field energy. The source of this magnetic field energy originates from the kinetic energy of electrons which migrate from cathode to anode. The induced electric field $E_{in}(t)$, which may accelerate charged particles in a high-energy state, is expressed as

$$E_{in}(t) \approx \frac{d}{dt}(LI) = L\frac{dI}{dt} + I\frac{dL}{dt} , \tag{1}$$

where L is the system inductance and I is the plasma current. The accelerating voltage due to the term LdI/dt has been investigated in previous studies.[3] In this report, we will concentrate on the accelerating mechanism due to the term IdL/dt. Change of the system inductance dL/dt is caused by the abrupt change of pinch radius. During expansion, the charged particles are accelerated outwardly by a pressure gradient force. The plasma radius exhibits a parabolic function of time t. The change of the system magnetic flux is proportional to the plasma radius. The major inductance change occurs at the last stage $(R \sim R_0)$ of plasma expansion. Thus, in order to simplify the subsequent analysis, we can assume that the plasma radius expands abruptly from $R = R_p$ to $R = R_0$ at time $t = 0$. As shown in Fig. 1, a highly collimated electron flux is generated on axis after expansion.

The electric field E in the pinch region is given by

$$E = V/d_p , \tag{2}$$

for $t < 0$ and for $t \to \infty$. Here V is the anode-cathode voltage difference. The steady-state current density before and after expansion is expressed as

$$J_0(r) = \begin{cases} \hat{J}_p = I_0/\pi R_p^2, & 0 < r < R_p \\ 0 & \text{otherwise} \end{cases} \tag{3}$$

for $t < 0$ and

$$J_0(r) = \begin{cases} \hat{J}_0 = I_0/\pi R_0^2, & 0 < r < R_0 \\ 0 & \text{otherwise} \end{cases} \tag{4}$$

for $t > 0$. We also assume that the current density is proportional to the electric field. That is,

$$J = \sigma E , \tag{5}$$

where σ is a constant depending on the cathode material, shape, etc.

The Ampere's law in the Maxwell equation is expressed as

$$\nabla \times \underline{B} = \frac{1}{c}\frac{\partial}{\partial t}\mathbf{E} + \frac{4\pi}{c}\mathbf{J}_T , \tag{6}$$

where the term proportional to $(1/c)(\partial \mathbf{E}/\partial t)$ is negligibly small. The total current density $\mathbf{J}_T$ in Eq. (6) represents both the steady-state value $J_0(r)$ and the transient density $J_{in}^t(r,t)$, which is related to the vector potential $A_z(r,t)$ by

$$J_{in}^t(r,t) = -\frac{\sigma}{c}\frac{\partial}{\partial t}A_z(r,t) , \tag{7}$$

where use has been made of Eq. (5) and the definition of the induced axial electric field

$$E_{in}(r,t) = -(1/c)(\partial/\partial t)A_z(r,t) .$$

Substituting Eq. (7) into Eq. (6) and making use of $B_\theta = \partial A_z(r,t)/\partial r$, we obtain

$$\frac{1}{r}\frac{\partial}{\partial r}\left[r\frac{\partial}{\partial r}A_z(r,t)\right] = -\frac{4\pi}{c}J_0(r) + \frac{4\pi\sigma}{c^2}\frac{\partial}{\partial t}A_z(r,t) , \tag{8}$$

for $t > 0$. Obviously, the solution to Eq. (8) is a combination of the steady-state and time-transient solutions. That is,

$$A_z(r,t) = A_{z0}(r) + \int_0^\infty dk\, A_k(r)\exp(-\lambda_k^2 t) , \tag{9}$$

where λ_k is the decay constant.

The transient solution $A_k(r)$ in Eq. (9) can be found by substitution of Eq. (9) into Eq. (8). After straightforward algebra, we obtain

$$\frac{1}{r}\frac{d}{dr}\left[r\frac{d}{dr}A_k(r)\right] + \frac{4\pi\sigma}{c^2}\lambda_k^2 A_k(r) = 0 , \tag{10}$$

for the transient solution. The physically acceptable solution to Eq. (10) is

$$A_k(r) = a_k J_0(kr) , \tag{11}$$

where $J_0(x)$ is the zeroth-order Bessel function of the first kind and the perpendicular wave number k is related to the decay constant λ_k by

$$\lambda_k = kc/(4\pi\sigma)^{1/2} . \tag{12}$$

Note that the solution $A_z(r,t)$ in Eq. (9) is equal to the steady-state solution $A_z(r)$ for $t < 0$. That is,

$$A_z(r, t < 0) = A_z(r, t = 0_+) ,$$

where $0_+ = \lim_{\delta \to 0} 0 + \delta$. Thus the coefficient a_k is related to the difference of the steady-state vector potentials before and after expansion, which is expressed as

$$\int_0^\infty dk\, a_k J_0(kr) = \Delta A_z(r) , \tag{13}$$

where $\Delta A_z(r)$ is approximately given by

$$\Delta A_z(r) = \begin{cases} \dfrac{2I_0}{c}\ln\left[\dfrac{R_0}{R_p}\right], & 0 < r < R_p \\[2ex] \dfrac{2I_0}{c}\ln\left[\dfrac{R_0}{r}\right], & R_p < r < R_0 \\[2ex] 0 & \text{otherwise.} \end{cases} \tag{14}$$

Multiplying both sides of Eq. (13) by $rJ_0(kr)$ and making use of the orthogonality of the Bessel function

$$\int_0^\infty x\,dx J_0(\eta x)J_0(\xi x) = \frac{\delta(\xi - \eta)}{\xi} ,$$

we obtain

$$a_k = \frac{2I_0}{ck}[J_0(kR_p) - J_0(kR_0)] . \tag{15}$$

The induced electric field

$$E_{in}(r,t) = -\frac{1}{c}\frac{\partial}{\partial t}A_z(r,t)$$

is obtained from Eq. (9) and is given by

$$E_{in}(r,t) = \frac{I_0}{2\pi\sigma}\int_0^\infty dk\, k[J_0(kR_p)-J_0(kR_0)]$$
$$\times J_0(kr)\exp(-\lambda_k^2 t)\ . \tag{16}$$

Defining

$$I = \frac{c^2 t}{\pi\sigma R_p^2}\ , \tag{17}$$

and carrying out the integration over k space in Eq. (10), the induced electric field in Eq. (16) is expressed as

$$E_{in}(r,t) = \frac{I_0}{\pi\sigma R_p^2\tau}\left[\exp\left[-\frac{R_p^2+r^2}{\tau R_p^2}\right]I_0\left[\frac{2r}{\tau R_p}\right]\right.$$
$$\left.-\exp\left[-\frac{R_0^2+r^2}{\tau R_p^2}\right]I_0\left[\frac{2R_0 r}{\tau R_p^2}\right]\right]\ . \tag{18}$$

The induced electric field in Eq. (18) is one of the main results in this work and can be used to investigate properties of the accelerating voltage for a broad range of system parameters. Note from Eq. (18) that the induced electric field $E_{in}(r,t)$ and the induced current density $J_{in}(r,t)=\sigma E_{in}(r,t)$ are maximum at the axis $(r=0)$ and decrease as the value r increases. At the axis of the plasma column $(r=0)$, the induced electric field in Eq. (18) is considerably simplified to

$$E_{in}(0,t) = \frac{I_0}{\pi\sigma R_p^2\tau}\left[\exp\left[-\frac{1}{\tau}\right]-\exp\left[-\frac{R_0^2}{\tau R_p^2}\right]\right]\ , \tag{19}$$

which is further simplified to

$$E_{in}(0,t) = \frac{I_0}{\pi r R_p^2\tau}\exp\left[-\frac{1}{\tau}\right] \tag{20}$$

for $R_0/R_p\gg 1$. The condition $R_0/R_p\gg 1$ can be easily satisfied in the present experiments. For simplicity of the present article, the analysis in the remainder of this report is restricted to the case of $R_p/R_0\ll 1$ and $r=0$, which corresponds to Eq. (20).

The total voltage difference $V_T(\tau)$ across the pinch region is the sum of the steady-state value V and the induced voltage $E_{in}d_p$. Defining the normalized value $v(\tau)=V_T(\tau)/V$, we obtain

$$v(\tau) = 1 + \frac{I_0 d_p}{\pi\sigma R_p^2 V}\frac{1}{\tau}\exp\left[-\frac{1}{\tau}\right]\ , \tag{21}$$

which has its maximum

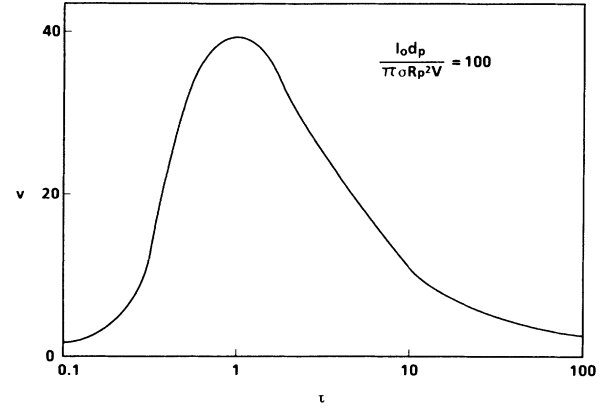$$v_m = v(\tau=1) = 1 + \frac{I_0 d_p}{\pi\sigma R_p^2 V}\exp(-1) \tag{22}$$

at

FIG. 2. Plot of normalized electron acceleration energy vs τ obtained from Eq. (21) for $R_0/R_p\gg 1$ and $I_0 d_p/\pi\sigma R_p^2 V=100$.

$$\tau=1\ . \tag{23}$$

Shown in Fig. 2 is the plot of the normalized accelerating voltage $v(\tau)$ versus τ obtained from Eq. (21) for $I_0 d_p/\pi\sigma R_p^2 V=100$. From Fig. 2, we note that the accelerating voltage is many times the anode-cathode voltage for $I_0 d_p/\pi\sigma R_p^2 V=100$. It is also noted from Fig. 2 that there are rising and falling portions of the accelerating voltage. From Eq. (24), we obtain the time

$$t_m = \frac{\pi\sigma R_p^2}{c^2}\ , \tag{24}$$

which corresponds to the maximum accelerating voltage V_m. In a typical present experiment, t_m is less than a fraction of a nanosecond. We therefore conclude that the peak accelerating voltage occurs right after expansion.

III. ENERGY SPECTRUM

It is also very useful to define the electron-energy spectrum $\mathscr{E}(v)$ by

$$\mathscr{E}(v)\Delta v = I\Delta t\ , \tag{25}$$

where I is the electron current. In obtaining Eq. (25), we have assumed that most of the pinch current is carried by electrons. In this context, we define the normalized energy spectrum $E(v)$ by

$$E(v) = \frac{v}{|dv/d\tau|}\ , \tag{26}$$

where use has been made of the fact that the current density profile at $r=0$ is the same as $v(\tau)$. The energy spectrum defined in Eq. (26) is a dimensionless parameter and provides a relative scaling. Note that Eq. (26) is defined in terms of the current density at the axis. Strictly speaking, the energy spectrum must be proportional to the total current as shown in Eq. (25). In this sense the energy spectrum in Eq. (26) is an approximate representation, which is, however, reasonable for the purpose of the present article.

Obviously, the time-integrated energy spectrum $E(v)$ consists of sum of the two contributions, one from the rising portion of the accelerating voltage and the other from the falling portion of the accelerating voltage. They are

$$E_1(v) = \frac{v}{v-1} \frac{\tau^2}{1-\tau}, \quad 0 \le \tau < 1$$

$$E_2(v) = \frac{v}{v-1} \frac{\tau^2}{\tau-1}, \quad 1 < \tau < \infty \ . \tag{27}$$

Therefore, the energy spectrum $E(v)$ is given by

$$E(v) = E_1(v) + E_2(v) \ . \tag{28}$$

We remind the reader that, making use of Eq. (26), the normalized time τ in Eq. (27) is explicitly determined in terms of the energy v for a specified value of the parameter $I_0 d_p / \pi \sigma R_p^2 V$. Shown in Fig. 3 is a plot of the energy spectrum versus v obtained from Eqs. (27) and (28) for $I_0 d_p / \pi \sigma R_p^2 V = 100$. In this figure, the logarithmic vertical scale represents a relative intensity in an arbitrary unit. Obviously, the energy spectrum in Eq. (28) has a singular point at $v = v_m$.

The highly collimated electron flux at the axis interacts with the dense-anode plasma, generating high-energy x-ray radiation and creating high-density microplasmas. Assuming that the anode plasma density is comparable with the density of a solid material, we can obtain the hard x-ray spectrum $\mathcal{S}(\varepsilon)$ from[4]

$$\mathcal{S}(\varepsilon) = \frac{1}{\varepsilon} \int_\varepsilon^{v_m} dv \frac{E(v)}{\sqrt{v}} \ln \left| \frac{1 + \sqrt{1 - \varepsilon/v}}{1 - \sqrt{1 - \varepsilon/v}} \right| , \tag{29}$$

where ε represents the hard x-ray energy normalized by

FIG. 4. Plot of the x-ray spectrum vs normalized x-ray energy ε obtained from Eq. (29) for parameters identical to Fig. 2.

eV. Here, V is the anode-cathode voltage difference. Substituting Eqs. (27) and (28) into Eq. (29) and making use of eq. (21), we can qualitatively estimate the hard x-ray spectrum emitted from anode plasma. It must be difficult to compare specific experimental data with the estimated values from Eq. (29) because of too many unknown physical parameters. But this estimated x-ray spectrum may provide a qualitative understanding of hard x-ray emission from a vacuum spark discharge. Nevertheless, we present in Fig. 4 a plot of the x-ray spectrum versus the x-ray energy ε obtained from Eq. (29) for $I_0 d_p / \pi \sigma R_p^2 V = 100$. The maximum normalized x-ray energy in Fig. 4 is $\varepsilon_m = 37.6$ for $I_0 d_p / \pi \sigma R_p^2 V = 100$, which corresponds to the maximum electron energy. Obviously, the high-energy tail of the x-ray spectrum exhibits nonthermal distribution. After a rough estimation, we find that the x-ray spectrum of the superthermal radiation in Fig. 4 is expressed as

$$\mathcal{S}(\varepsilon) = c\varepsilon^{-3.3} \tag{30}$$

in the x-ray energy range $10 \le \varepsilon < 30$. In Eq. (30), c is a constant. Finally, we conclude this section by pointing out that the superthermal x-ray spectrum in Eq. (30) is very similar to that obtained from experimental data presented in Ref. 7.

IV. DISCUSSION

In this paper, we have developed a theoretical model based on the magnetic field diffusion in order to explain complex vacuum spark phenomena, including emission of superthermal x radiation. As shown in Fig. 5, the plasma radius R reaches its minimum value R_p (pinch radius) at
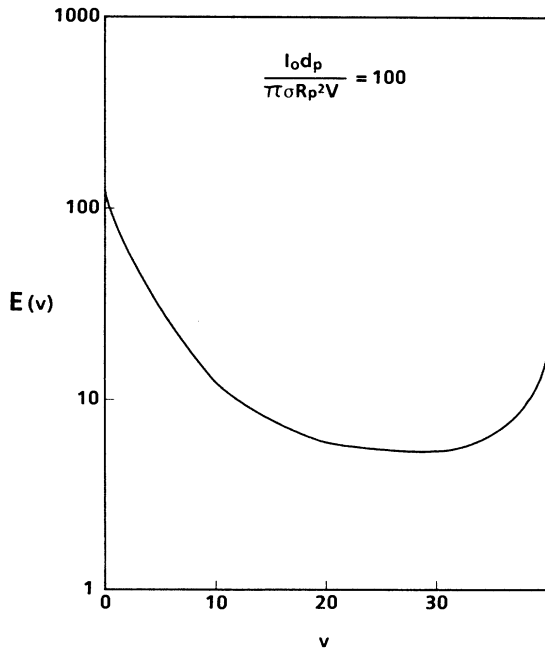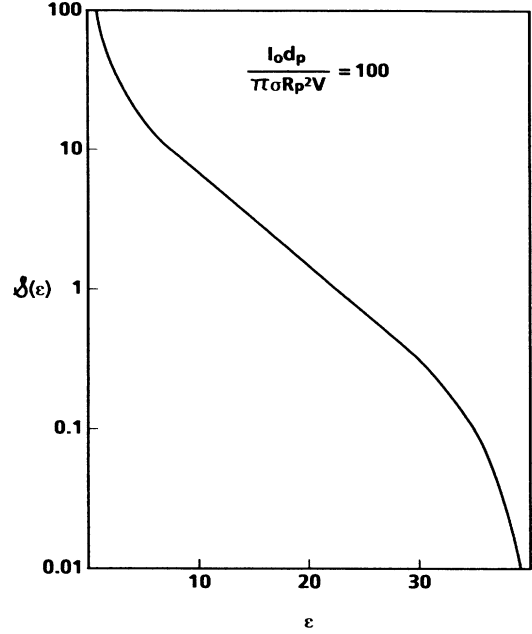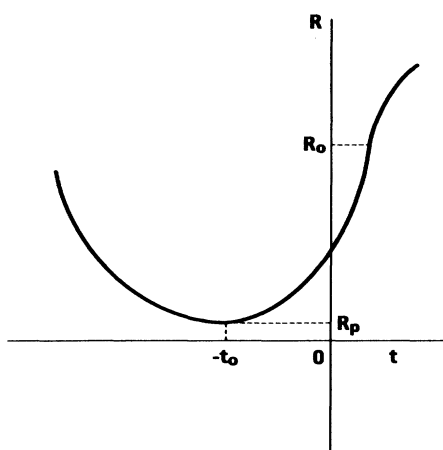

FIG. 3. Plot of the energy spectrum vs the normalized energy v obtained from Eq. (28) for parameters identical to Fig. 2.

FIG. 5. Schematic presentation of plasma column radius R vs time t.

$t = -t_0$ and then expands to $R = R_0$ at $t = 0$. During constriction of the plasma column, the inductance of the plasma system increases, thereby storing magnetic field energy. Assuming that the plasma current is constant, the plasma expansion from $R = R_p$ to $R = R_0$ means a change of the system inductance, thereby ensuring intense induced accelerating voltage. The plasma expansion is caused by the pressure gradient force. Thus the plasma radius may be a parabolic function of time t. Since the change of the system magnetic flux is proportional to the plasma radius, it is reasonable to conclude that the major inductance change occurs at the last stage

of plasma expansion $(R \sim R_0)$. In order to make the analysis simple, we therefore assume that the plasma radius expands abruptly from $R = R_p$ to $R = R_0$ at $t = 0$ as shown in Fig. 5. The delay time t_0 of the expansion after the pinch is in the order of 10 ns.

Once the plasma column expands abruptly at $t = 0$, the magnetic field stored inside the pinched plasma diffuses, creating an intense induced electric field [Eq. (18)]. This induced electric field has its peak value on axis and rapidly decreases as the radial coordinate r increases. Obviously, the induced electric field accelerates charged particles into a very-high-energy state. The induced plasma current is proportional to the induced electric field as shown in Eq. (5). Therefore, high-energy electron flux is well collimated on axis. This highly collimated electron flux interacts with the dense-anode plasma, thereby generating high-energy x-ray radiation and creating high-density microplasmas. The high-current electron beam interacting with a dense plasma could also induce a current-driven ion-acoustic instability. The high-energy x-ray source is therefore the high-density microplasmas, in agreement with recent experimental observation.[5] In addition, this high-energy x radiation occurs at the delay time t_0 after the pinch state. Very often, high-energy electron flux may also drill a small hole in the anode.[6] This qualitative discussion may provide a reasonable theoretical basis to explain various observations in the present vacuum spark experiments.[1,7]

ACKNOWLEDGMENTS

[1]V. A. Veretennikov, S. N. Polukhin, O. G. Semenov, and Yu. V. Sidelnikov, Fiz. Plazmy 7, 1199 (1981) [Sov. J. Plasma Phys. 7, 656 (1981)].

[2]J. W. Sheares, Phys. Fluids 19, 1426 (1976).

[3]J. Fukai and E. J. Clothiaux, Phys. Rev. Lett. 34, 863 (1975), and references therein.

[4]W. Heitler, The Quantum Theory of Radiation (Oxford University Press, Oxford, England, 1954).

[5]T. N. Lee (unpublished).

[6]W. A. Cilliers, R. U. Datla, and H. R. Griem, Phys. Rev. A 12, 1408 (1975).

[7]T. N. Lee, Ann. N.Y. Acad. Sci. 251, 112 (1975).